

Late-State Ripening Dynamics of a Polymer/Clay Nanocomposite

Xiaoliang Wang,[†] Pingchuan Sun,^{*,‡} Gi Xue,^{*,†} and H. Henning Winter^{*,§}

[†]Department of Polymer Science and Engineering, Nanjing University, Nanjing 210093, China, [‡]Key Laboratory of Functional Polymer Materials, Ministry of Education, College of Chemistry, Nankai University, Tianjin 300071, China, and [§]Department of Chemical Engineering and Department of Polymer Science and Engineering, University of Massachusetts, Amherst, Massachusetts 01003

Received July 28, 2009; Revised Manuscript Received January 11, 2010

ABSTRACT: A remarkably simple viscoelastic relaxation pattern was found for a physical gel that, beyond its gel point, slowly ripens toward a stable structural state. The material is a nanocomposite that consists of two components, an organoclay and an end-functionalized polymer, which get mixed at prescribed ratio. When freshly combined, the polymer intercalates into the clay galleries and eventually exfoliates the clay. The exfoliation occurs without applying flow. The nanocomposite quickly passes through the gel point and, with increasing ripening time, t_r , its characteristic modulus $G_c(t_r)$ and relaxation time $\lambda_c(t_r)$ grow and decay by orders of magnitude, respectively. Surprisingly, their product, $G_c(t_r)\lambda_c(t_r)$, is found to remain constant during the two vastly different structuring processes of intercalation and exfoliation. For the rheological experiments, $G_c(t_r)\lambda_c(t_r) = \text{constant}$ means that dynamic mechanical data can be merged into each other by log/log shifting under 45°.

1. Introduction

Nonequilibrium phenomena are pervasive in multicomponent, solid materials throughout the spectrum of materials applications, including pharmaceuticals, ion conductors for photovoltaic systems, personal care products, and gel-based drug delivery and tissue culture formulations. The internal structure of such *man-made* solid materials is rarely equilibrated, as they are not given sufficient time to ripen and/or the ripening process arrests before reaching equilibrium due to a free-energy landscape with multiple local minima.^{1–4} Nonequilibrium states determine not only the manufacturing and processing of these materials but also their end-use. The understanding of materials away from equilibrium has been recognized as one of the grand challenges to science and engineering.⁵ In spite of the importance of such out-of-equilibrium materials, relatively little is known that could help to control the dynamics of structure development or tailor the structure for specific purposes. We therefore selected a model composite material with constituents that slowly connect into a disordered, three-dimensional structure and used rheology to study the evolving out-of-equilibrium states while approaching a stable end-state.

We use small-amplitude oscillatory shear to follow the growth of internal connectivity during the structural ripening process. The low-frequency dynamic moduli, $G'(\omega, t)$ and $G''(\omega, t)$, are known to be especially sensitive measures of connectivity of internal structure. However, any data point on these curves can represent the ripening process as long as the G' and G'' curves maintain their general shape and can be shifted into a single pair of curves. Here we will represent the shifting through a characteristic modulus and a characteristic relaxation time

$$G_c(t) = \lim_{\text{low } \omega} G'(t) \quad \text{and} \quad \lambda_c(t) = 1/\omega_x(t) \quad (1)$$

*To whom correspondence should be addressed: Tel 1.413.5450922; Fax 1.413.5451647; e-mail winter@ecs.umass.edu.

During ripening in the solid state, the modulus grows and the relaxation time decays as shown schematically in Figure 1.

The characteristic modulus G_c denotes the low-frequency plateau value of G' , which is a typical rheological property of ideal solids in the zero limit, $\omega \rightarrow 0$. Physical gels and soft glassy materials are not solids in this ideal sense since they can relax when given sufficient time which might be extremely long. However, physical gels behave as solids in a wide experimental time window, which includes a plateau modulus G_c at low frequencies. This is meant when taking the limit at “low ω ” in eq 1 instead of taking the ultimate limit $\omega \rightarrow 0$. The relaxation at extremely long times is outside the experimental window of this study and will not be discussed here.

Throughout this study, the characteristic relaxation time, λ_c , is defined as inverse of the crossover frequency, ω_x , for which $G' = G''$, and is chosen because it is a distinct and measurable point on the modulus curves. A more meaningful choice as reference time would be the longest relaxation time if it were measurable unambiguously. For this study we prefer the crossover time as reference because of its accessibility.

The model system is thought to be representative for groups of physical gels and soft glasses that share the phenomenon of a slowly equilibrating structure when subjected to a jump in environment.^{6,7} Typically, the structure has not fully matured at the gel point and the long-time modulus keeps growing as shown in Figure 1. The longest relaxation time, which had diverged at the gel point, decays again as the structure continues to ripen. While much is known about the rheology at the gel point and its distinct power-law spectrum,^{8,9} no specific viscoelasticity pattern seems to be known for the evolving nonequilibrium states beyond the gel point. These late ripening stages are the focus of this study.

There have been indications that a general ripening pattern might exist beyond the gel point. Such expectation is based on the observation that similar master curves, through rescaling, represent the time-dependent rheology of such diverse materials as cross-linking epoxies,¹⁰ physical gelation of PVC plastisols,¹¹

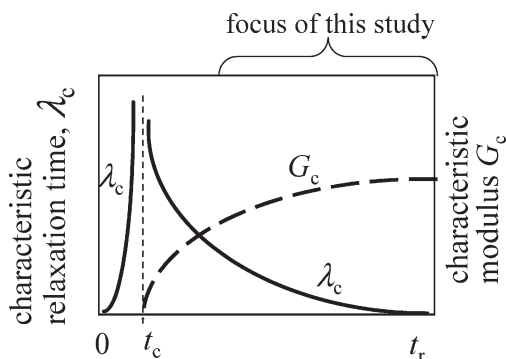


Figure 1. Rheology of physical gelation, schematically. Parameter is the ripening time, t_r . Shown are a characteristic modulus after the gel point, G_c , and a characteristic longest relaxation time, λ_c , before and after t_c (see definition in eq 1). The early liquid-to-solid transition, marked by a diverging longest relaxation time at the gel point, t_c , is fairly well understood. Most of the structural development in physical gels and soft glasses, however, occurs in the solid state where slow structural ripening dominates. This study addresses the question whether G_c and λ_c are related to each other.

aging of colloidal suspensions with weakly attractive particles,¹² Laponite clay suspensions,^{13–18} and surface aggregation. This suggests that, when applying such scaling methods to our model material, a general framework of ripening dynamics might become apparent through the experimental findings with a model material.

We have recently reported a new class of gel-like telechelic polymer/exfoliated-clay nanocomposites using an end-functionalized polymer and highly anisotropic, organically modified silicates.^{19–22} Polymer/clay interactions not only enhance the clay dispersion, intercalation, and eventual exfoliation but also result in a sample spanning network structure.^{23–26} In the following, we will study the viscoelastic properties of the evolving structure of such a model physical gel with random clay orientation and rescale the data in search of a systematic rheological pattern beyond the gel point. We are mostly concerned with the time dependence of the rheological properties. The stable end-state (after a sufficiently long ripening period) serves as reference in the data analysis. Reproducibility is guaranteed by avoiding shear-induced orientation.

2. Materials and Experimental Procedure

Materials. The end-functionalized polymer is a dicarboxyl-terminated 1,4-polybutadiene oligomer (CTPB) with $M_n = 4200$ (Aldrich Chemical). CTPB is a fluid at room temperature which is advantageous for the performing the ripening experiments (no solvent needs to be added). The organoclay (C₁₈-clay) was prepared as follows: 10.0 g of industrially purified pristine montmorillonite (Tianjin Organic Clay Corp. China, cation exchange capacity is 1 mequiv/g) was dispersed into 1000 mL of distilled water at 87 °C for cation exchange with 3.5 g (equal to 1 mequiv/g) of octadecyltrimethylammonium chloride (denoted as C18A) for 12 h. The processed clay was washed with distilled water and checked with a 0.1 N AgNO₃ solution for residual Cl[−] ions. After the washing, the organoclay was dried at 87 °C for 12 h before use. The process was described in detail elsewhere.¹⁹ The purpose of the C18A macrocounterions is to neutralize charge on the clay surfaces, to open the clay galleries, and to provide a thermodynamically compatible environment for the diffusion of the matrix molecules.

Sample Preparation. Organoclay/CTPB nanocomposites were prepared by gently and quickly mixing prescribed amounts of clay and CTPB in a disposable vial at ambient temperature (15–20 °C) as described by Zhu et al.²⁰ In our previous work we showed that no obvious orientation of clay sheets appeared

during the mixing process.^{20,21} While maintaining quiescent conditions, the structure ripens into a stable clay dispersion as has been demonstrated previously.²¹ The ripening process begins after having mixed the clay into the CTPB (at $t_r = 0$). The freshly mixed sample undergoes a liquid-to-solid transition (physical gelation) very early since the initially aggregated clay particles already have sufficient surface area for the sticky matrix macromolecules to attach and to connect the tactoids into a sample-spanning network structure.⁶ The early evolving relaxation pattern resembles gelation.⁸ However, its liquid-to-solid transition is only the beginning of the structural evolution. The molecules slowly swell the clay particles by diffusing into the clay galleries, a widely studied process that is called “intercalation”. As further molecules keep diffusing into the galleries, the spacing of the clay sheets increases until they get so far apart that sheets cease to interact directly and begin to diffuse independently. This disintegration of the clay particles leads to a stable exfoliated clay (denoted as “SEC” in the following) structure with large-scale concentration fluctuations of randomly oriented, individual clay sheets throughout the polymer matrix.^{19–21} The model system naturally ripens into a SEC nanocomposite when heated up to a certain temperature (> 80 °C). The existence of SEC as final, stable, and path-independent structure with unique rheology was confirmed experimentally for samples of this study. Exfoliation without applying shear flow is possible for a concentration of up to 10 wt %, and we use 8 wt % clay in this study to ensure a final exfoliated structure. SEC might be close to equilibrium, but no attempt will be made here to find an ideal thermodynamic equilibrium.

Rheometry. The rheological measurements were performed on a strain-controlled rotational rheometer (ARES of TA Instruments Corp.). Cone-and-plate geometry of 50 mm diameter and 0.04 rad cone angle were chosen to ensure uniform shear throughout the samples. As measurement criterion, the strain amplitude was kept within the linear viscoelasticity region while being large enough for obtaining reasonable signal intensities in the frequency range (0.01–100 rad/s) and temperature range (26–116 °C). The temperature dependence of the dynamic storage modulus (G') and loss modulus (G'') was measured at frequencies (ω) of 1 rad/s and in the temperature range from 26 to 116 °C with a heating rate of 2 K/min. Dynamic mechanical data during ripening were generated with a sequence of frequency sweeps between 100 and 0.2 rad/s^{8,27,28} and interpolated with the IRIS tools.²⁹ To prevent the degradation of the samples, all the rheological experiments at elevated temperatures were performed under the protection of nitrogen gas.

Structure Characterization. TEM was carried out on a JEM 2100 electron microscope operated at 200 kV. Samples for TEM were cut into ultrathin sections with a diamond knife at a temperature of −90 °C using a LKB2008 microtome. Microtomed thin sections were mounted on copper grids without staining. The TEM image (Figure 2) suggests that most of the clay sheets are disorderly dispersed in the polymer matrix after 12 h annealing at 80 °C.

3. Results and Discussion

Mechanical spectroscopy is able to measure the distribution of relaxation times and strengths of the material structure. The sample is exposed to small-amplitude oscillatory shear, $\dot{\gamma}(t) = \dot{\gamma}_a \sin(\omega t)$, while measuring the in-phase and out-of-phase contribution of the oscillating shear stress response, $\sigma(t) = G' \dot{\gamma}_a \sin(\omega t) + G'' \dot{\gamma}_a \cos(\omega t)$, and hence defining the storage modulus G' and loss modulus G'' .³⁰ The period of the experiment, $t_p = 2\pi/\omega$, selectively probes relaxation processes with relaxation times in the order of $\tau \approx t_p$. Large structural units require large relaxation times and vice versa. Correspondingly the long relaxation times of long-range connectivity in the gel will be especially visible in low frequency (i.e., long relaxation time) measurements.

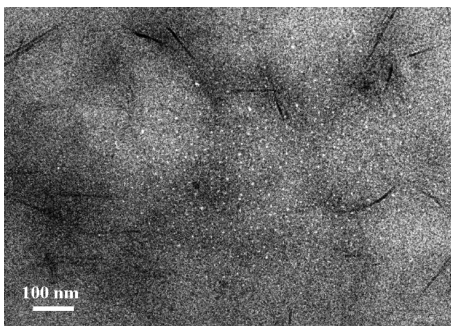


Figure 2. TEM of the 8 wt % C18/CTPB nanocomposite after having been annealed for 12 h at 80 °C.

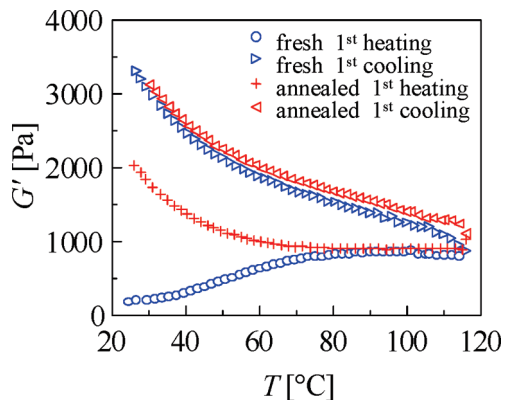


Figure 3. Temperature sweep of CTPB/C₁₈-clay 8 wt %. Comparison of freshly mixed and annealed samples for 12 h at room temperature. $\omega = 1$ rad/s, heating and cooling at 2 K/min. The samples were heated and then cooled. The annealed sample starts out with a partially developed structure.

Dynamic mechanical data during ripening were generated with a sequence of frequency sweeps between 100 and 0.2 rad/s. Repetition of the multifrequency test³¹ while the sample is changing leads to an extensive G' , G'' data set with each data point belonging to a new state of the material. Interpolation of the data results in “snapshots” $G'(\omega, t_r)$, $G''(\omega, t_r)$ of the material’s viscoelasticity at distinct ripening times, t_r . The IRIS software²⁹ provides convenient and accurate interpolation of the time-resolved measurements. This time-resolved rheometry method²⁷ was originally developed to study gelation, but it is ideally suited for an experimental study of out-of-equilibrium materials with time-dependent connectivity.

The experiments are in contrast to single frequency tests, which lack the information for a complete scaling analysis. The reason is the decay of the characteristic relaxation time scales of the evolving solid structure and the need for reducing the time scale of observation, ω^{-1} , accordingly. Otherwise, each data point would belong to a new material-defined frequency, $\omega\lambda_c(t_r)$, and scaling would not be meaningful. Single-frequency scans, however, are useful for a quick test as will be shown next.

Accelerated Ripening at Elevated Temperature. A single-frequency heating scan demonstrates the accelerated ripening at increased temperature (see Figure 3). A freshly mixed sample was compared to a sample that was allowed to slowly ripen at 26 °C for 12 h after mixing. The storage modulus (G') of the freshly mixed sample steadily increased upon heating from 26 to 80 °C. G' increased further upon cooling with a final value that was 18 times its value before heating. G' of the 12 h annealed sample was already 11 times higher than G' of the freshly mixed sample (at 26 °C). G' softened with increased temperature from 26 to 50 °C as expected from a

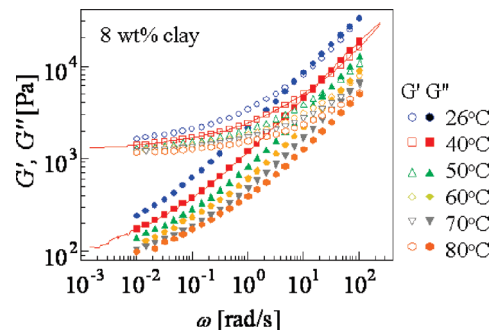


Figure 4. Temperature dependence of dynamic moduli of the stable exfoliated clay (SEC) structure that had been reached through heating to 120 °C for 20 min. The continuous lines mark G' and G'' master curves at 40 °C (reference temperature for data in Figure 8).

polymeric material. When heated beyond 50 °C, its G' began to increase until it leveled off at about 80 °C. Both annealed and freshly mixed sample exhibit the same G' and G'' after that heat treatment. These observations suggest that SEC with the same stable structure has established itself independently of the path of the ripening process.

Viscoelasticity of the Exfoliated State (SEC). $G'(\omega)$ and $G''(\omega)$ of the SEC are shown in Figure 4. The G' master curve levels off at low frequencies. The G'' upturn of the low frequencies indicates the existence of a very slow relaxation mode as expected for a physical gel. However, this very slow mode is outside the experimental window (not shown here). The structure is stable over a wide temperature range and can be characterized rheologically with classical time–temperature superposition methods. The horizontal shift factor, a_T , follows the typical WLF pattern, and the vertical shift, b_T , can be expressed with Ferry’s rubber elasticity term for polymers ($b_T = \rho_0 T_0 / \rho T$).³⁰ With a temperature “scaling ratio”

$$n_T = (\log b_T) / (\log a_T) \approx 0 \quad (2)$$

the temperature shift for the SEC is horizontal. The well-defined reference state provides the framework for describing the rheological consequences of the evolving connectivity. G' and G'' during ripening can now be scaled by shifting to the corresponding SEC moduli. The limiting values of the characteristic relaxation time, $\lambda_{c,\infty}(T) = \lim_{t_r \rightarrow \infty} \lambda_c(t_r, T)$, and the low-frequency modulus, $G_{c,\infty}(T) = \lim_{t_r \rightarrow \infty} G_c(t_r, T)$, serve as scaling parameters.

Time-Resolved Rheometry of Ripening Dynamics. Time-resolved dynamic mechanical data at $T = 40$ °C and $T = 80$ °C are shown in Figure 5. Equivalent data were obtained at $T = 26, 50, 60,$ and 70 °C. Interpolation of these data leads to the “snapshots” in Figure 6. At all temperatures of this study, the transition from liquid to solid occurred nearly instantaneously (~ 100 s at 40 °C) so that most of the ripening happened beyond the gel point in the solid state. The typical solid behavior can be recognized by a $\tan \delta$ (at low frequencies) which increases with frequency ω (not shown here).

Scaling of the Ripening Dynamics. Two independent parameters govern the isothermal ripening experiments: the ripening time t_r and the temperature T . Scaling was attempted here with respect to these two parameters and with respect of the SEC moduli, $G'_\infty(\omega, T)$ and $G''_\infty(\omega, T)$. We began with the rescaling of isothermal $G', G''(\omega, t_r, T)$ data at discrete “ripening times” $t_{r,1}$, $t_{r,2}$, and $t_{r,3}$. Surprisingly, the shape of G' and G'' curves did not change significantly during

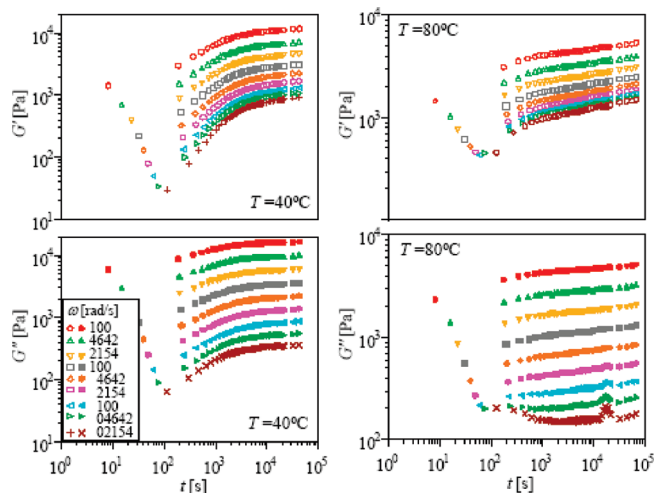


Figure 5. Isothermal ripening experiments for a freshly mixed 8 wt % clay/polymer nanocomposite at 40 °C (left) and 80 °C (right). Time-resolved dynamic modulus data strings belong to constant frequencies $\omega = 100, 46.42, 21.54, 10.0, 4.642, 2.154, 1.00, 0.4642,$ and 0.2154 rad/s, the top string belonging to the highest and the bottom string belonging to the lowest frequency. Corresponding measurements at 26, 50, 60, and 70 °C gave similar looking results.

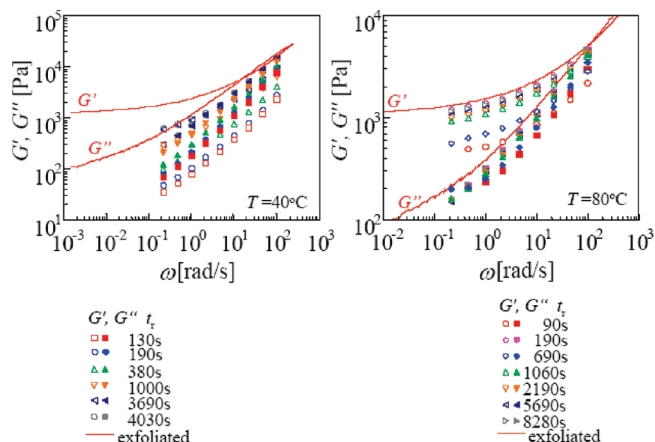


Figure 6. Evolution of dynamic moduli during isothermal ripening. The snapshot data at discrete ripening times were generated by interpolation of the data in the previous figure. The SEC master curves at $T = 40$ °C and $T = 80$ °C are shown in comparison (continuous lines). The plot shows only 25% of the data so that individual curves can be recognized.

isothermal ripening so that they could be collapsed onto the corresponding SEC curve (see Figure 7a)

$$\begin{aligned} G_{\infty}'(\omega, T) &= b_r G'(\omega a_r, t_r, T); \\ G_{\infty}''(\omega, T) &= b_r G''(\omega a_r, t_r, T) \end{aligned} \quad (3)$$

The scaling of G', G'' data is based on relaxation processes that are fairly slow, as observed in oscillatory shear at low or intermediate frequencies, since this study is mostly concerned with the long-range connectivity of the evolving network structure as represented by the slow modes. High-frequency data follow other scaling relations, which are not pursued here. The low-frequency scaling defines the horizontal and vertical “ripening shift” factors, $a_r = a_r(t_r, \infty, T)$ and $b_r = b_r(t_r, \infty, T)$, respectively. The bracket (t_r, ∞) denotes the “ripening shift” between an intermediate state, t_r , and SEC, $t_r \rightarrow \infty$.

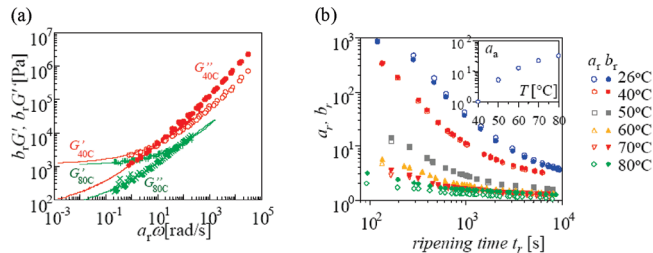


Figure 7. Ripening of 8 wt % clay in CTPB: (a) G', G'' data of Figure 5 after interpolating according to the time-resolved rheometry procedure²⁷ and shifting onto the SEC master curve (lines). For comparison, the corresponding G', G'' data of ripening at 80 °C is added. The difference between the two data sets (40 °C vs 80 °C) is due to the temperature dependence as shown in Figure 4. (b) Shift factors for horizontal and vertical shift with SEC as reference, open symbols for a_r and filled symbols for b_r . Most of the corresponding data points sit on top of each other. The magnitude of $(a_r - 1)$ or $(b_r - 1)$ is a measure of the “distance” from the SEC. Inset: the acceleration shift factor, a_a , that merges all curves into the single shift function of Figure 8.

Interesting for this study is the specific physical meaning of the shift functions. The horizontal shift defines the reduction of the characteristic time $\lambda_c(t_r)/\lambda_{c,\infty}$, and the vertical shift defines the increase of the characteristic modulus, $G_c(t_r)/G_{c,\infty}$

$$a_r(t_r; \infty; T) = \frac{\lambda_c(t_r, T)}{\lambda_{c,\infty}(T)}; \quad 1/b_r(t_r; \infty; T) = \frac{G_c(t_r, T)}{G_{c,\infty}(T)} \quad (4)$$

Both time shift a_r and the modulus shift b_r approach unity at very long times when the structure has ripened to its SEC state. The ripening “scaling ratio”

$$n_r = (\log b_r)/(\log a_r) \quad (5)$$

defines the slope of the rescaling of the dynamic data ($n_r = 1$ for shift at 45°).

The most surprising finding from our experiments is also shown in Figure 7b: The two ripening shift functions a_r and b_r were found to be equal (scaling ratio $n_r \approx 1$) for ripening experiments at elevated temperatures ($T = 40, 50, 60,$ and 70 °C). Only for ripening at 26 and 80 °C, a_r and b_r deviate slightly from each other. This means that the product of characteristic modulus and relaxation time

$$G_c(t_r, T)\lambda_c(t_r, T) \approx G_{c,\infty}(T)\lambda_{c,\infty}(T) \quad (6)$$

stays constant throughout most of the ripening process ($G\lambda = 360$ Pa s at $T = 40$ °C).

4. Heuristic Model of Ripening Dynamics

The ripening dynamics accelerates at elevated temperatures but the shape of the ripening shift factors seems to be temperature invariant (see Figure 7b). A horizontal shift along the ripening time axis is sufficient to merge; in a reasonably good approximation, all relaxation data into a single master curve for the entire ripening dynamics (Figure 8), $f(a_r t_r, T) = b_r(t_r; \infty; T_{\text{ref}}) = a_r(t_r; \infty; T_{\text{ref}})$. The ripening acceleration factor, a_a , as shown in Figure 7b, inset, can be expressed as Taylor expansion $a_a(T; T_{\text{ref}}) = 1 + \alpha(T - T_{\text{ref}}) - \beta(T - T_{\text{ref}})^2$. Above $T = 40$ °C, the quadratic term of the acceleration factor is small, $\alpha(T - T_{\text{ref}}) \ll \beta(T - T_{\text{ref}})^2$, within the experimental region. The ripening function, as a quantitative measure of the distance from SEC, decays rapidly at first and continues very slowly. This suggests a sequence of two distinctly different mechanisms which may be expressed in an empirical ripening function

$$f(t_r, T) - 1 = (f_0 - 1) \left\{ \left(\frac{t_{r,0}}{t_r} \right)^{-2} + \left(\frac{t_{r,0}}{t_r} \right)^{-1/2} \right\} \quad (7)$$

with parameters $f_0 = 2.6$ and $t_{r,0} = 54.5$ s (at $T = 40$ °C). The overlay of this function together with the data is shown in Figure 8. All experiments condense into a single scaling relation. The ripening function decays to value 1, $\lim_{t_r \rightarrow \infty} f(a_r t_r, T) = 1$, at long times because of SEC being the reference state.

5. Discussion

One of the objectives of this study is the formation of a nanocomposite that is random with respect to its clay orientation. This needs to be emphasized since, as separate rheological experiments in preparation of this study have shown, shear-induced clay orientation is not able to relax back into randomness even after extremely long annealing times. Rheologically, this expresses itself in a low modulus due to a reduced internal connectivity of the oriented clay–polymer network. Data will depend on specific stain histories. To avoid this, it is important that we start out with a sample of random orientation and preserve randomness during the mixing of clay into the polymer. We take advantage of the fact that the clay by itself consists of aggregates in which clay particles (stacks of aligned day sheets) are randomly assembled and that randomness is protected as long as the aggregate state is preserved. Keeping this in mind, we mixed clay and polymer under mild shearing conditions without breaking the clay aggregates. The mixing was distributive but at low stress. Unbroken aggregates are noticeable by the opaque appearance of the nanocomposite sample after mixing. Within an hour after mixing, the sample becomes optically clear due to the polymer-induced breaking of the clay aggregates into the small clay particles. Macroscopic randomness is maintained at these early ripening stages since the randomly oriented clay particles are still assembled as stacks of clay sheets. This provides the random initial condition for our experimental study of the structural ripening. Exfoliation times are orders of magnitude larger than the breakup time of aggregates in the presence of end-functionalized polymer. The time-resolved rheological experiments involve only small shear strains so that the randomness of the clay sheets is maintained. All results of this study refer to randomly oriented clay structures. Oriented clay structures will be studied separately.

A uniform representation of ripening at all temperatures is possible because the material assumes a stable end-state which can serve as reference for the structure development. As an alternative, we could have rescaled the experimental observations with the critical gel state³² as has been done before for characterizing materials near the gel point.^{10,33} However, physical gels or soft glasses exhibit liquid-to-solid transition states that are not unique. Their critical gel state depends on the experimental path^{34,35} and possibly on the connectivity of trapped intermediate states. This problem of path dependence is avoided by rescaling the ripening dynamics with the stable end state (SEC) as defined above.

The shift factors of Figure 7b express the distance of the ripening structure from SEC. We could easily reach SEC at temperatures above 80 °C but only could see how closely the structure approaches SEC when ripening at 70, 60, 50, 40, and 26 °C. We also performed an extremely long experiment at 40 °C; however, it could not reach SEC within 3 days. We ascribe this to large energy barriers at temperatures below 50 °C. The shifting of entire modulus curves into a master curve requires that the shape of all curves remains constant during the ripening process. This is the case for relaxation modes throughout an intermediate frequency range. More experiments are needed to quantify the frequency limits of this behavior.

For colloidal nanocomposites, the diffusion of polymer molecules into the clay galleries and, at later stages, diffusion of exfoliated clay leaves are known to be governed by several

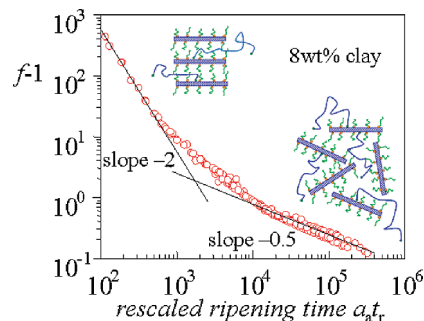


Figure 8. Ripening function as defined in eq 7 is dominated by two processes: fast intercalation and slow exfoliation. The reference temperature is $T_{\text{ref}} = 40$ °C.

competing processes and phase behavior.^{14–16,36} Cocard et al. found the shear modulus to continue to evolve and a stable state was not reached after having passed the gel point of gelling Laponite clay suspensions.¹³ The loss modulus of the gel increased at low frequencies, indicating the presence of slow relaxation processes. This complexity makes it even more surprising that a single function is able to describe the overall change in rheology. The specific shape of the scaling function of Figure 8 is sample specific. However, in spite of the fundamental difference of these two structuring processes, suspension-type structure followed by an exfoliated leaf structure, the property $G_c(t_r) \cdot \lambda_c(t_r) = \text{constant}$ is found for the entire structure evolution beyond the gel point. This indicates that $G_c \lambda_c = \text{constant}$ might be more widely found with other complex materials during structural ripening. Many more experiments on other physical gels and soft glasses will be required to define the range of validity. The experimentally found scaling ratio value of unity, $n_r = 1$, is so specific that it will be interesting to see whether other physical gels exhibit the scaling property but require another n_r value.

The property $G_c(t_r) \lambda_c(t_r) = \text{constant}$ has consequences for the modeling of viscoelasticity of physical gels and soft glasses. These need to be explored further. An example is the complex viscosity. The product $G \lambda$ is property of a solid but has the dimension of a viscosity. For $n_r = 1$, the complex viscosity, $\eta^*(\omega)$ or $\eta^*(G^*)$, shifts horizontally during the ripening process:

$$\frac{b_r}{a_r} \eta^*(a_r \omega, t_r, T) \approx \eta^*(\omega, T) \quad \text{or} \quad \frac{b_r}{a_r} \eta^*(b_r G^*, t_r, T) \approx \eta^*(G^*, T) \quad (8)$$

This is shown in Figure 9 for four ripening states and the shift onto SEC. η^* is finite for liquids and solids. Different from the steady shear viscosity, η^* does not diverge at the liquid-to-solid transition (except for its low- G^* limit or its low- ω limit). G^* is chosen here as abscissa since it magnifies differences between material states.^{37,38}

The frequency-dependent moduli shift without changing their shape. That means that the relaxation time spectrum for an early structural state and its corresponding relaxation time spectrum of the final structural state, when written in discrete form

$$G(t, t_r, T) = \sum g_i(t_r, T) e^{-t/\lambda_i(t_r, T)},$$

$$G_\infty(t, T) = \sum g_{i,\infty}(T) e^{-t/\lambda_{i,\infty}(T)} \quad (9)$$

are related through

$$\lambda_i(t_r, T) = a_r(t_r; \infty; T) \lambda_{i,\infty}(T);$$

$$g_i(t_r, T) = g_{i,\infty}(T) / b_r(t_r; \infty; T) \quad (10)$$

It should be noted that this shifting property belongs to the observed frequency window and that there are upper and lower

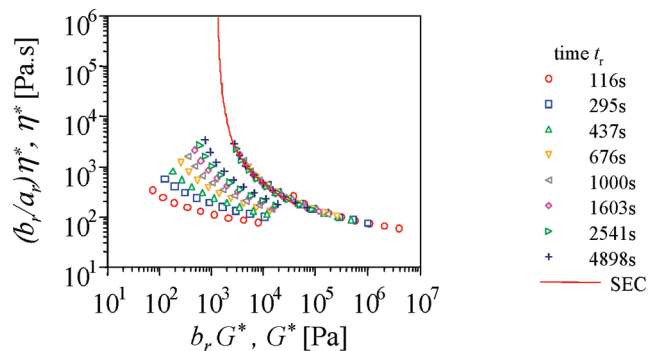


Figure 9. Complex viscosity at increasing ripening states and merged into a master curve at the reference temperature. The shift is horizontal because of an n_r value of 1. The reference temperature is $T_{\text{ref}} = 40^\circ\text{C}$. For comparison, the viscosity of the pure matrix fluid is 22 Pa s at $T_{\text{ref}} = 40^\circ\text{C}$.

limits of the proposed dynamics, which need to be explored further.

6. Conclusions

The sample preparation method is ideally suited for preparing nanocomposites of random clay orientation. The random clay/polymer system (with 8 wt % clay) reached its most stable structure independently of the experimental path (using three different protocols), which is a prerequisite for using it as reference. The liquid-to-solid transition (gel point), which can be recognized by its power-law relaxation modulus, $G(t) = St^{-n}$, occurs very quickly after mixing the clay into the polymer. The consecutive ripening in the solid state evolves in a stunningly regular pattern with distinct properties that have never been observed before to our knowledge. Surprisingly, the product of characteristic modulus and time, $G_c \lambda_c$, stays constant throughout the ripening process while both properties by themselves undergo large change. All low-frequency experiments collapse into a single scaling relation with a sequence of two pronounced power-law regions: a fast ripening process ($\sim t_r^{-2}$) followed by slow ripening ($\sim t_r^{-1/2}$). The ripening time, t_r , is the independent parameter, which defines the state of ripening and projects the time necessary to reach the stable exfoliated clay (SEC) state. The experimental protocol of this study is ideally suited for characterizing materials with time-dependent structure in general and for exploring the range of validity of the new findings for a wider class of colloidal solids.

Acknowledgment. H.H.W. acknowledges the support of NSF CBET 0651888. The study was supported by National Natural Science Foundation of China (Grants 20774041, 20825416, and 20904020), the China Postdoctoral Science Foundation, and Jiangsu Planned Projects for Postdoctoral Research Funds.

References and Notes

- (1) Stradner, A.; Sedgwick, H.; Cardinaux, F.; Poon, W. C. K.; Egelhaaf, S. U.; Schurtenberger, P. *Nature* **2004**, *432*, 492.
- (2) Sciortino, F.; Mossa, S.; Zaccarelli, E.; Tartaglia, P. *Phys. Rev. Lett.* **2004**, *93*, 4.
- (3) Dijkstra, M.; Hansen, J. P.; Madden, P. A. *Phys. Rev. Lett.* **1995**, *75*, 2236.
- (4) Ovarlez, G.; Coussot, P. *Phys. Rev. E* **2007**, *76*, 011406.
- (5) Fleming, G. R.; Ratner, M. A. *Phys. Today* **2008**, *61*, 28.
- (6) King, H. E.; Milner, S. T.; Lin, M. Y.; Singh, J. P.; Mason, T. G. *Phys. Rev. E* **2007**, *75*, 20.
- (7) Giannelis, E. P.; Krishnamoorti, R.; Manias, E. *Adv. Polym. Sci.* **1999**, *138*, 107.
- (8) Winter, H. H.; Mours, M. *Adv. Polym. Sci.* **1997**, *134*, 165.
- (9) Nijenhuis, K. T. *Adv. Polym. Sci.* **1997**, *130*, 1.
- (10) Adolf, D.; Martin, J. E. *Macromolecules* **1990**, *23*, 3700.
- (11) Kakiuchi, M.; Aoki, Y.; Watanabe, H.; Osaki, K. *Macromolecules* **2001**, *34*, 2987.
- (12) Trappe, V.; Weitz, D. A. *Phys. Rev. Lett.* **2000**, *85*, 449.
- (13) Cocard, S.; Tassin, J. F.; Nicolai, T. *J. Rheol.* **2000**, *44*, 585.
- (14) Mourchid, A.; Delville, A.; Lambard, J.; Lecolier, E.; Levitz, P. *Langmuir* **1995**, *11*, 1942.
- (15) Mourchid, A.; Delville, A.; Levitz, P. *Faraday Discuss.* **1995**, *275*.
- (16) Mourchid, A.; Levitz, P. *Phys. Rev. E* **1998**, *57*, R4887.
- (17) Awasthi, V.; Joshi, Y. M. *Soft Matter* **2009**, *5*, 4991.
- (18) Shukla, A.; Joshi, Y. M. *Chem. Eng. Sci.* **2009**, *64*, 4668.
- (19) Chen, T. H.; Zhu, J. J.; Li, B. H.; Guo, S. Y.; Yuan, Z. Y.; Sun, P. C.; Ding, D. T.; Shi, A. C. *Macromolecules* **2005**, *38*, 4030.
- (20) Zhu, J. J.; Wang, X. L.; Tao, F. F.; Xue, G.; Chen, T. H.; Sun, P. C.; Jin, Q. H.; Ding, D. T. *Polymer* **2007**, *48*, 7590.
- (21) Wang, X. L.; Gao, Y.; Mao, K. M.; Xue, G.; Chen, T. H.; Zhu, J. J.; Li, B. H.; Sun, P. C.; Jin, Q. H.; Ding, D. T.; Shi, A. C. *Macromolecules* **2006**, *39*, 6653.
- (22) Wang, X. L.; Tao, F. F.; Xue, G.; Zhu, J. J.; Chen, T. H.; Sun, P. C.; Winter, H. H.; Shi, A. C. *Macromol. Mater. Eng.* **2009**, *294*, 190.
- (23) Ray, S. S.; Okamoto, M. *Prog. Polym. Sci.* **2003**, *28*, 1539.
- (24) Pinnavaia, T. J.; Beale, G. W. *Polymer-Clay Nanocomposites*; Wiley: New York, 2000.
- (25) Balazs, A. C.; Singh, C.; Zhulina, E. *Macromolecules* **1998**, *31*, 8370.
- (26) Sinsawat, A.; Anderson, K. L.; Vaia, R. A.; Farmer, B. L. *J. Polym. Sci., Part B: Polym. Phys.* **2003**, *41*, 3272.
- (27) Mours, M.; Winter, H. H. *Rheol. Acta* **1994**, *33*, 385.
- (28) Winter, H. H.; Chambon, F. *J. Rheol.* **1986**, *30*, 367.
- (29) Winter, H. H.; Mours, M. *Rheol. Acta* **2006**, *45*, 331.
- (30) Ferry, J. D. *Viscoelastic Properties of Polymers*, 3rd ed.; John Wiley & Sons: New York, 1980.
- (31) Holly, E. E.; Venkataraman, S. K.; Chambon, F.; Winter, H. H. *J. Non-Newtonian Fluid Mech.* **1988**, *27*, 17.
- (32) Vilgis, T. A.; Winter, H. H. *Colloid Polym. Sci.* **1988**, *266*, 494.
- (33) DeRosa, M. E.; Mours, M.; Winter, H. H. *Polym. Gels Networks* **1997**, *5*, 69.
- (34) Horst, R. H.; Winter, H. H. *Macromolecules* **2000**, *33*, 130.
- (35) Horst, R. H.; Winter, H. H. *Macromolecules* **2000**, *33*, 7538.
- (36) Bousmina, M. *Macromolecules* **2006**, *39*, 4259.
- (37) Booi, H. C.; Palmen, J. H. M. In *Moldenaers, P., Keunings, R., Eds.; Theoretical and Practical Rheology*; Elsevier: Brussels, 1992; p 321.
- (38) Winter, H. H. *Rheol. Acta* **2009**, *48*, 241.